Computational Materials Science 242 (2024) 113097

Contents lists available at ScienceDirect

Computational Materials Science

journal homepage: www.elsevier.com/locate/commatsci

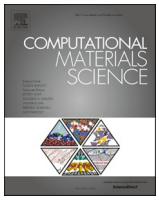

Full Length Article

Formation and growth of transition metal carbides in ferrite

R.J. Slooter [a,*], M.H.F. Sluiter [a], W.G.T. Kranendonk [b], C. Bos [a,b]

[a] Department of Materials Science and Engineering, Delft University of Technology, Mekelweg 2, 2628 CD Delft, the Netherlands
[b] Tata Steel, 1970 CA IJmuiden, the Netherlands

ARTICLE INFO

Keywords:
Nano-precipitate
Ab initio
Atomistic simulation
Guinier-Preston zone
Ferrite

ABSTRACT

Carbide nano-precipitates are commonly used to improve mechanical properties of steel. It has been experimentally observed that TiC, NbC, and VC carbide precipitates initially form as 'plate-like' particles oriented in the {1 0 0} planes of the ferrite lattice. These platelets share similarities with Guinier-Preston zones in Al-Cu alloys.

The clustering of group IV and V transition metal atoms (M = Ti, Zr, Hf, V, Nb, Ta) in ferrite is studied using density functional theory. It is deduced that the transition metal carbides all form in a similar way. Furthermore, the transition from an initial M–C cluster to a NaCl-structured platelet to a NaCl-structured precipitate is examined through atomistic simulations using Modified Embedded Atom Method potentials. A route is established along which transition metal carbides form and transform into precipitates that possess the Baker-Nutting orientation relation with the ferrite matrix.

1. Introduction

Nano-precipitates perform a key role to increase the mechanical hardness of micro-alloyed steels. The number and size-distribution of precipitates are commonly modelled using classical nucleation and growth theory (CNGT) [1–4]. These CNGT models provide a good insight in average precipitation behavior. Conventional CNGT treats the formation of precipitates as compact particles with regular shapes, such as spheres, ellipsoids, cubes, etc. Furthermore, CNGT does not account for the variation of properties, such as composition, among precipitates of different sizes. However, transmission electron microscopy (TEM) reveals that various carbides in the bcc-Fe (α) matrix are not compact particles, rather they grow initially as platelets in {1 0 0} planes [5–8] that evolve to spheroids as they grow larger. Moreover, the stoichiometry of metal carbides 'MC' (where M = Ti, V, or Nb) is found to be size dependent [6,8–10]. Previous simulations for NbC and TiC [11] have demonstrated that the formation of MC precipitates involves a precursor state. Both simulations and experiments suggest that this precursor state is akin to a 'Guinier-Preston' (GP)-like zone [8,11], which eventually transforms into the final NaCl-structured MC precipitate.

In the same study [11] the precursor stage for Nb and Ti carbides is found to have an ordered $FeMC_3$ structure, stable up to the 1100 K range. Relations between the binding energies of M–M and M–C pairs embedded in ferrite and the nature of the cluster, where Fe and M atoms initially form a checkerboard pattern, were identified from simulations using Modified Embedded Atom Method (MEAM) [12,13] potentials and from Density Functional Theory (DFT) calculations. In this work the study of these pairs is expanded for multiple group IV and group V transition metals. Similarities are identified between Ti, Zr, Hf, V, Nb, and Ta behavior in ferrite. As for most transition metals there is no available MEAM potential (where M = Ti, Zr, Hf, V, Nb, Ta) we perform DFT calculations on multiple M–M and M–C pairs. Additionally some M–M–M triplets are calculated. From these DFT calculations we find that all the corresponding MC carbides seem to form via the same mechanism, where the MC carbides form a precursor stage with its M atoms in a single $(1\,0\,0)_\alpha$ plane of the ferrite matrix.

Our previous study [11] also shows that the precursor stage $FeMC_3$ clusters do not have the NaCl-structure that is observed for larger precipitates, and which is known to be the most stable bulk structure [14]. The $FeMC_3$ clusters rather display a checkerboard pattern for the Fe and M atoms in a single $(1\,0\,0)_\alpha$ plane. The transformation of a $FeMC_3$ cluster to a NaCl-structured platelet is studied here using MEAM [12,13] potentials in LAMMPS [15]. Various steps in the transformation are identified, where the $FeMC_3$ cluster displays similarities in behavior to the GP zone in aluminum alloys. The attraction of vacancies to the cluster occurs in the same manner as the GP zone in aluminum alloys [16], where vacancies aid transport of precipitate forming atoms toward the GP zone as vacancies are bound to the M atoms. In the simulations the

* Corresponding author.
E-mail address: R.J.Slooter@tudelft.nl (R.J. Slooter).

https://doi.org/10.1016/j.commatsci.2024.113097
Received 13 February 2024; Received in revised form 7 May 2024; Accepted 8 May 2024
Available online 20 May 2024

role of vacancies and their interaction with the $FeMC_3$ clusters are also studied. Using atomistic simulations the main driving force behind the transformation from the initial cluster to the NaCl-structured platelet has been investigated. It is established that the main driving force is the strain in the planes perpendicular to the habit plane of the initial cluster.

First the methodology is presented in Section 2, then in Section 3 the results of the DFT calculations are presented and discussed. In Section 4 the transformation mechanism is studied and discussed.

2. Methodology

2.1. Introduction

In this work both DFT calculations and MEAM LAMMPS simulations are performed. The DFT calculations are used for small systems in which a pair of M atoms, or a pair consisting of a M atom and a C atom is embedded in ferrite. This shows whether the formation of a specific pair is energetically favorable compared to fully dissolved atoms, i.e., in the infinitely diluted limit. These calculations show how initial clusters can form from the solid solution. As DFT calculations are computationally demanding only small supercells are constructed.

For larger systems LAMMPS is used to perform atomistic simulations on $FeMC_3$ clusters. The atomistic simulations are specifically used to establish how a $FeMC_3$ cluster can transform to a NaCl-structured platelet and eventually a multilayered NaCl-structured precipitate.

2.2. DFT calculations

The DFT calculations are performed using projector-augmented wave (PAW) pseudo potentials as implemented in the Vienna Ab initio Simulation Package (VASP 5.3.5) [17–21].

For both M–M and M–C pairs the binding energy $E_{bind.}$ at 0 K is investigated where a positive value indicates attraction and a negative energy indicates repulsion. The binding energy is defined as:

$$E_{bind.} = iE(Fe) + j\Delta E(M) + k\Delta E(C) - E\left(Fe_iM_jC_k\right), \quad (1)$$

where $\Delta E(X)$, with $(X = M, C)$, is the solute excess energy given by:

$$\Delta E(X) = E(Fe_iX) - iE(Fe). \quad (2)$$

Here $E(Y)$ is the total energy of a supercell containing Y (where $Y = Fe_pM_qC_r$). Each supercell contains a bcc lattice, the lattice parameter is fixed at 2.833 Å which is the equilibrium lattice parameter for pure bcc Fe, hereby also fixing the supercell volume.

For different M–M, and M–C pairs embedded in bcc Fe a simulation is performed in a $3 \times 3 \times 3$ unit bcc and a $4 \times 4 \times 4$ bcc unit supercell, containing 54 and 128 substitutional atom sites respectively. For the $3 \times 3 \times 3$ supercell we use 6k-points along all axes, the k-points are arranged following a regular Γ-centered mesh. The electronic wave functions are expanded in terms of plane waves, for all supercells a cutoff kinetic energy set at 400 eV was used. For the $4 \times 4 \times 4$ supercell we use 4k-points along all axes, again using the regular Γ-centered mesh. For both the $3 \times 3 \times 3$ bcc unit and $4 \times 4 \times 4$ bcc unit supercell the precision is set to medium. The structural relaxation convergence criterium for energy is that the total energy change between subsequent ionic iterations is smaller than 0.1 meV, and for forces that the norms of each force is smaller than 100 meV/nm.

Additionally some pairs are also simulated in a $5 \times 5 \times 5$ bcc unit supercell, containing 250 substitutional atom sites. Apart from the supercell size the same settings as for the $4 \times 4 \times 4$ bcc unit supercell are used. Again 4k-points were used following a regular Γ-centered mesh.

2.3. LAMMPS simulations for the transformation mechanism

The transformation from initial M–C clusters to a NaCl-structure is studied using Modified Embedded Atom Method (MEAM) potentials in LAMMPS (v 3mar20) [15]. In these simulations the MEAM potentials for the Fe-Nb-C [13] and Fe-Ti-C [12] ternary systems are used.

First the solute excess energy for a C atom at an octahedral interstitial site is established using Eq. (2), as well as the solute excess energy for replacing an Fe atom with a M (=Nb,Ti) atom. Using these solute excess energies the binding energies can be calculated for the various clusters using Eq. (1). Here it is explicitly assumed that C atoms only occupy octahedral interstitial sites, and M atoms only occupy substitutional sites on the bcc lattice. The initial clusters are of a $FeMC_3$ type, as presented in [11]. Note that the (total) binding energy contains both a chemical energy and an elastic energy component.

Clusters are simulated in a $20 \times 20 \times 20$ or a $40 \times 40 \times 20$ bcc unit cell supercell, where the supercell-size effects are negligible as the results for a cluster between the two supercells differ less than 0.01 eV/atom for the M and C atoms within the cluster. A constant volume is used where we use the equilibrium lattice parameter, $a = 2.8636$ Å, for bcc Fe from the MEAM potentials [12,13]. The relaxations are performed at 0 K, where the stopping criteria are set such that the energy change between iterations is $1 \bullet 10^{-8}$ eV, for forces the 2-norm of the global force vector must be less than 100 meV/nm, i.e., no force component on any atom is larger than 100 meV/nm. To illustrate the transformation from an $FeMC_3$ cluster to a NaCl-structured precipitate clearly, clusters with a square shape are used. However, the effects presented in Section 4 also hold true for simulations performed with both rectangular and more circular clusters.

3. DFT calculations for the formation of transition metal clusters in ferrite

To investigate the general trends in metal-carbide formation DFT calculations are performed for group IV and V transition metals embedded in a bcc iron lattice. Various M–M, M–C pair configurations are simulated: Fig. 1 gives a schematic overview of the pair configurations. The simulated pairs are chosen to include several close pairs that would exist in the NaCl-structure or the $FeMC_3$ clusters found in [11].

The M–M pair configurations are labelled by their occupied sites indicated by roman numerals in Fig. 1, where all other bcc lattice sites are occupied by Fe atoms. For the M–C pair configurations a M atom is located at the site indicated by a roman numeral, and a C atom at the integer numbered site. Note that the I-VII M–M pair in the $3 \times 3 \times 3$ bcc unit supercell also contains the I-II pair for periodic boundaries, so it is not included in the results. The calculated binding energies for group IV metals are presented in Table 1, and for the group V metals in Table 2.

For the pairs given in Tables 1 and 2 the same trend is seen for the binding energy, again a positive value indicates attraction and a negative energy indicates repulsion. We remark that the change from a $3 \times 3 \times 3$ unit cell to a $4 \times 4 \times 4$ unit cell supercell largely preserves the order of favorability of the pairs. Additionally the change in M–M pair binding energies is less than 0.05 eV in most cases, for M–C pairs the change is less than 0.25 eV with one exception, namely the I-5 pair for vanadium. Given that the magnitude of the changes is largely similar within each species we do not expect significant changes in the order of favorability when using a larger supercell.

It must be noted that the binding energies of the least unfavorable pairs in the group V transition metals are only slightly negative. Therefore the I-IV and I-V M–M pairs are simulated again in a $5 \times 5 \times 5$ bcc unit cell sized supercell to see if the pairs are really repulsive or in fact attractive. As in a larger supercell the supercell-size effect caused by the boundaries is reduced for the relaxation, the relaxations are performed at constant volume from an initially 'perfect' bcc lattice.

In Tables 1-3 it is shown that generally the I-IV pair is the most favorable for M–M pairs, however for Ti and V the I-V pair is slightly more favorable than the I-IV pair. The most favorable M–C pair is the I-2 pair for all metals except vanadium for the $4 \times 4 \times 4$ supercell. There are some differences between the two groups of transition metals. Within

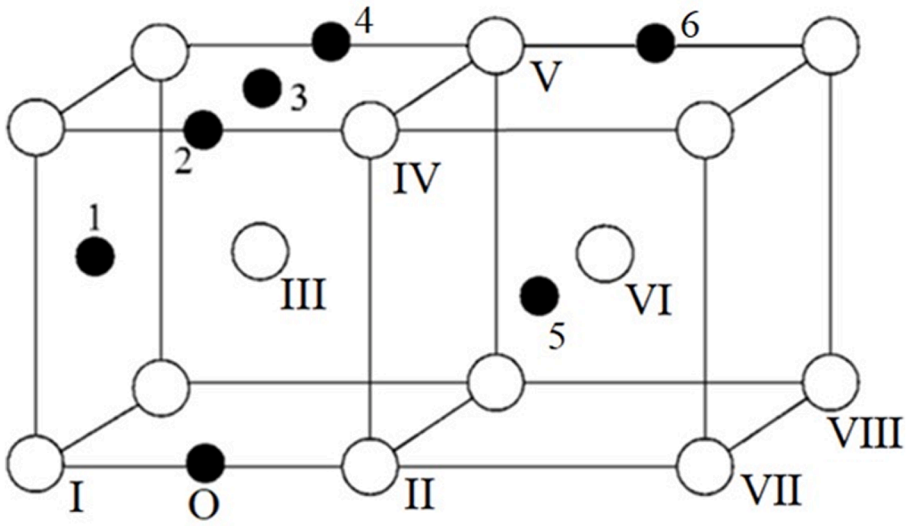

Fig. 1. Positions of atom pairs, each pair is labelled by the sites the M or C atoms occupy. Corresponding binding energies are given in Tables 1 and 2. M atoms are placed at the sites with Roman numerals, and C atoms are placed at the integer numbered sites.

Table 1
Binding energies for various M–M and M–C pairs for group IV transition metals. The pairs indicated are illustrated in Fig. 1, all binding energies are given in eV. The binding energy for the most favorable (or least unfavorable) M–M pair, and the most favorable M–C pair is printed bold.

	Ti		Zr		Hf	
Supercell size	3 × 3 × 3	4 × 4 × 4	3 × 3 × 3	4 × 4 × 4	3 × 3 × 3	4 × 4 × 4
M–M pair	$E_{bind.}$ [eV]					
I-II	−0.143	−0.136	−0.216	−0.126	−0.128	−0.128
I-III	−0.237	−0.249	−0.449	−0.365	−0.453	−0.448
I-IV	0.007	−0.009	**−0.043**	**0.025**	**0.025**	**0.018**
I-V	**0.019**	**0.011**	−0.126	−0.049	−0.054	−0.051
I-VI	−0.047	−0.024	−0.114	−0.033	−0.108	−0.032
I-VII	–	−0.017	–	−0.015	–	−0.009
M–C pair	$E_{bind.}$ [eV]					
I-0	−0.817	−0.728	−1.578	−1.365	−1.484	−1.309
I-1	**0.012**	0.038	**0.011**	0.094	**0.057**	0.101
I-2	−0.022	**0.103**	−0.041	**0.179**	−0.004	**0.174**
I-3	−0.150	−0.027	−0.325	−0.092	−0.278	−0.094
I-4	−0.090	0.033	−0.186	0.023	−0.133	0.031
I-5	−0.080	0.041	−0.135	0.052	−0.091	0.057

Table 2
Binding energies for various M–M and M–C pairs for group V transition metals. The pairs indicated are illustrated in Fig. 1, all binding energies are given in eV. The binding energy for the most favorable (or least unfavorable) M–M pair and the most favorable M–C pair is printed bold.

	V		Nb		Ta	
Supercell size	3 × 3 × 3	4 × 4 × 4	3 × 3 × 3	4 × 4 × 4	3 × 3 × 3	4 × 4 × 4
M–M pair	$E_{bind.}$ [eV]					
I-II	−0.145	−0.125	−0.216	−0.170	−0.210	−0.164
I-III	−0.259	−0.239	−0.402	−0.393	−0.470	−0.449
I-IV	**−0.012**	−0.023	**−0.016**	**−0.006**	**−0.019**	**−0.008**
I-V	−0.019	**−0.012**	−0.053	−0.053	−0.059	−0.049
I-VI	−0.062	−0.033	−0.080	−0.040	−0.098	−0.044
I-VII	–	−0.036	–	−0.034	–	−0.028
M–C pair	$E_{bind.}$ [eV]					
I-0	−0.528	−0.479	−1.366	−1.209	−1.353	−1.195
I-1	−0.162	−0.139	−0.108	−0.059	−0.125	−0.074
I-2	−0.114	−0.001	**−0.103**	**0.070**	**−0.115**	**0.054**
I-3	−0.122	−0.014	−0.271	−0.097	−0.272	−0.094
I-4	**−0.096**	0.010	−0.142	0.018	−0.138	0.025
I-5	−0.393	**0.015**	−0.123	0.023	−0.127	0.031

the group IV metals attractive interactions are stronger, both for M–M pairs and M–C pairs, than in the group V metals.

Ti and V atoms behave different from the other metals, this is most likely a result of the size difference. The Ti and V atoms are both considerably smaller than the other M atoms in the same group when embedded in the ferrite matrix, so they have a better fit with the ferrite matrix [22]. This is also reflected by their comparatively low repulsion in the I-III M–M pair and the I-0 M-C pair. The size effect is also visible when comparing the lattice parameters of the various MC carbides, where the TiC and VC lattice parameter is smaller than for the other carbides which are relatively comparable [23].

In short, from the pair interactions we see two main contributions, elastic interaction contribution which derives from the atomic size differences with other substitutional atoms [22], and a chemical interaction contribution. The chemical contribution is observed from the differences between group IV and V transition metals, as there are noticeable differences between the calculated trends for both groups.

For the M–M and M–C pairs all metals display a roughly similar behavior for their pair interactions embedded in ferrite. This is true for M–C pairs in particular. In [11] the pair interactions for Ti and Nb atoms

Table 3
Binding energies for the most favorable (or least unfavorable) M–M and M–C pairs in Tables 1 and 2. Here a 5 × 5 × 5 bcc unit cell sized supercell is used to allow for better relaxation and less influence from the supercell boundaries. The most favorable pairs are printed in bold.

	Ti	Zr	Hf	V	Nb	Ta
M–M pair	$E_{bind.}$ [eV]					
I-II	−0.160	−0.089	−0.095	−0.169	−0.148	−0.138
I-IV	−0.016	**0.069**	**0.065**	−0.039	**0.026**	**0.024**
I-V	**0.010**	0.029	0.004	**−0.038**	−0.004	−0.001
M–C pair	$E_{bind.}$ [eV]					
I-1	0.093	0.168	0.178	−0.092	0.018	0.005
I-2	**0.128**	**0.208**	**0.207**	**0.007**	**0.102**	**0.091**

have been linked to the formation of a checkerboard pattern consisting of Fe and M atoms within a {1 0 0} plane, where the M and Fe atoms form an ordered cluster together with C atoms. As all the studied metals display the same (un)favored interactions for studied pairs and triplets it is plausible that all their carbides form via a similar path, like the path found in [11]. However, it cannot be ruled out that different, more

favorable, paths for Zr, Hf, V, and Ta carbides exist.

For further examination two M-C–C triplets are also of particular interest, as they had highly favorable binding energies in the simulations performed in [11]. Besides the M-C–C triplet several M–M–M triplets are studied to see which orientation is preferred, or least unfavorable. Results are given in Table 4. The results show that the M–M–M triplets in a single {1 0 0} plane are least unfavorable for all metals except for Ti and V. Furthermore the binding energies of the pairs that make up I-IV-VII and I-V-VII are roughly equal to the binding energy of the triplet, from this we deduce that the pair interactions provide a good first approximation for the binding energy of the M clusters. Hence the clusters formed by the substitutional atoms, without C atoms, can be predicted by looking at the pair interactions.

For the M-C–C triplets the binding energy of the triplet differs from the sum of binding energy for the pairs that make up the triplet as is displayed in Table 4, here the binding energies for the C–C pairs are taken from [11]. Note that the triplets where the C atoms are closer to the M atom are favored. It is observed that the triplets display the same preferential ordering. For the studied metals distinct trends are observed, hinting that the formation of M–C clusters may follow similar steps for all metals. The III-0–2 triplet contains a 0–2C–C pair, and two I-1 M-C pairs. The III'-0–3 triplet contains a 0–3C–C pair, a I-1 M-C pair, and I-2 M-C pair. Note that the site III' is the III site mirrored in the {1 0 0} plane containing the I, II, IV, and VII sites. In simulations using the MEAM potentials it has been shown that the formation of a Fe-M–C cluster is preceded by the clustering of C atoms [11], as the binding of M atoms to a pre-existing Fe-C cluster is more favorable than the clustering of M atoms in ferrite. At this scale the same preference for all investigated M atoms to attach to a C atom 'cluster' is observed. Nevertheless the interaction between M and C atoms is less predictable, so the exact energies cannot be inferred by summing pair interactions.

The DFT calculations show that the various transition metals display similar trends for their pair interactions within the bcc iron lattice, hinting that their carbides form in a similar manner, which is experimentally observed for TiC, VC, and NbC precipitates [5–8]. Additionally, simulations have previously shown that TiC and NbC carbides form following a similar path [11], where both the M–M and M–C pair interactions for both metals displayed similar trends.

4. Transformation mechanism

4.1. Transformation to NaCl-structure

Several M–C clusters are simulated using LAMMPS (v 3mar20) [15], with two separate MEAM potentials for the Fe-Nb-C [13] and Fe-Ti-C ternary systems [12] to simulate the transition path. The initial (Fe, M)-C cluster has a structure where the C atoms lie in the {2 0 0} plane adjacent to the {1 0 0} plane containing the M and Fe atoms. We will refer to the {1 0 0} plane containing the M atoms as the habit plane. The M and Fe atoms form a checkerboard-pattern in the habit plane. The structure of these clusters is presented in Fig. 2, the generalized chemical formula is $FeMC_3$ where additional C atoms can be located at the outer edge of the cluster, for brevity we will write $FeMC_3$. As there is a high Fe fraction present in the $FeMC_3$ clusters the interface between the cluster and the surrounding ferrite matrix is nearly perfectly coherent, it is observed that all simulated clusters (with a diameter up to 4.5 nm) retain a coherent interface. There are some specific features for the $FeMC_3$ cluster, also described in [11]:

- There are two types of C atoms; i) C atoms which lie in 'rows' where there are two C atoms (near an Fe site) on one side of the cluster, and ii) C atoms that lie 'between-rows'. These rows, ideally, lie alternating on both sides of the habit plane, which is displayed in Fig. 2c and 2d.
- Fe atoms in the cluster have three close C neighbors. Two of these lie within a 'row', the other C atom lies 'between-rows'. The Fe-C distance is roughly 1.85 Å for all three C atoms, hence the C atoms form a triangle as mentioned above. The Fe-C bonds are shown in Fig. 2e.
- The M atoms have 8 nearest Fe neighbors. These fall into two groups, the Fe atoms on the side of the in-row C atoms are pushed away from the M atom, whereas the other Fe atoms are pushed closer to the M atom. The Nb-Fe connections are shown in Fig. 2f.

The transition from the $FeMC_3$ cluster, as given in Fig. 2, to a MC precipitate with a NaCl-structure depends on the cluster size and does not occur for small clusters, as observed experimentally [6,8]. Notice that a single {1 0 0} plane in the bcc lattice is a {1 0 0} plane rotated by 45° in a fcc lattice. The NaCl-structure consists of two superposed fcc lattices, one being a M lattice and the other a C lattice. As mentioned, the $FeMC_3$ cluster has its M atoms in a single {1 0 0} plane, i.e., the habit plane, but the C atoms lie in the first adjacent {2 0 0} planes. The transition to a NaCl structure thus requires the movement of the C atoms, and the movement of M atoms. The M atoms can come from the solid solution, or move within the cluster itself. In Fig. 3 a schematic overview of the transformation is presented.

The C atoms move into the 'NaCl-sites', i.e., into the octahedral interstitials in the habit plane. The rearrangement of C atoms occurs around some of the Fe atoms in the habit plane, and may be preceded by the substitution of the Fe atom by a vacancy as the substitution of Fe atoms by vacancies is also energetically favorable, e.g., in Fig. 3 (step 2) for $FeNbC_3$ (in the 8×8 cluster) the movement of the C atoms increases the binding energy by 4 eV, only removing the Fe atom gains 1.5 eV, and both removing the Fe atom and moving the C atoms gains 5.7 eV, so the combination is most favorable (Table 5). We note that the increase in binding energy is very large for the 8×8 cluster, in practice these relatively large clusters would not retain their $FeNbC_3$ structure. The transformation is likely to occur in smaller clusters, as the increase in binding energy associated with the transformations is significant as shown in Table 5. The preference for both relocating C atoms, and replacing Fe atoms with vacancies indicates that vacancies can enhance the transformation speed as they incentivize the relocation of C atoms in the habit plane. Additionally, it is remarked that the clusters, for all sizes, act as strong vacancy attractors, cf. [11].

Additionally several of the C atoms in neighboring sites are pushed outward from the habit plane. These C atoms are still close to the $FeMC_3$ cluster and are still attracted to the cluster, however their binding energy is lowered making it easier for the C atoms to dissolve back into the matrix. These excess C atoms can then attach to other clusters, or reattach to the cluster at more favorable sites. We note a strong bond

Table 4
Binding energies for metal triplets embedded in the ferrite matrix, the triplets are based on the most favorable M−M pairs from Tables 1 and 2. In all cases a $4 \times 4 \times 4$ bcc unit cell supercell is used. The various configurations can be found in Fig. 1, except for III' which is the site where III is mirrored with respect to the {1 0 0} plane in which sites I, II, IV lie. The binding energy for the most favorable (or least unfavorable) triplet is printed bold. In the last two rows the difference in energy between the triplets and the pairs that can be found in the triplet are given, this shows that some triplets are favored over the pairs. Particularly for the group V metals there is a strong preference for the III-0–2 triplets over the various pair energies.

	Ti	Zr	Hf	V	Nb	Ta
M–M–M	$E_{bind.}$ [eV]					
I-IV-VII	−0.030	**0.025**	**0.015**	−0.076	**−0.059**	**−0.054**
I-IV-VIII	0.000	−0.065	−0.063	**−0.042**	−0.080	−0.074
I-V-VII	**0.008**	−0.123	–	−0.053	−0.140	−0.124
M-C–C	$E_{bind.}$ [eV]					
III-0–2	**0.177**	**0.304**	**0.313**	**−0.163**	**−0.008**	**−0.034**
III'-0–3	0.035	0.128	0.130	−0.165	−0.050	−0.071
$E_{bind.}$ triplet $-\sum(E_{bind.}$ pairs in triplet) [eV]						
III-0–2	0.071	0.086	0.081	0.085	0.080	0.084
III'-0–3	−0.111	−0.150	−0.150	−0.030	−0.066	−0.066

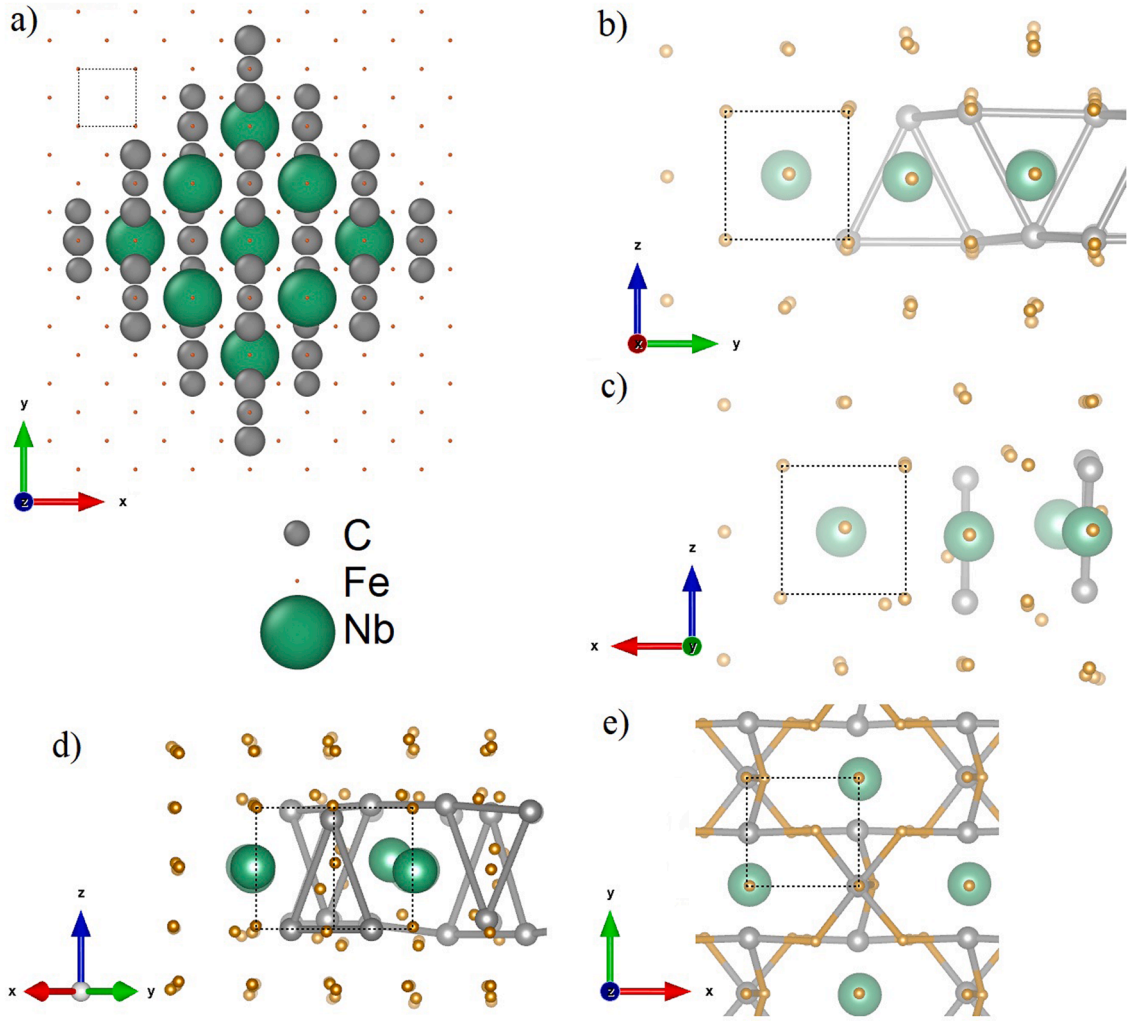

Fig. 2. The Initial $FeMC_3$ cluster illustrated for M = Nb, however for M = Ti the same cluster is found [11]. The small (brown) atoms are the Fe atoms, the large (green) atoms are the Nb atoms, and the mid-sized (gray) atoms are the C atoms. In a) a top-view of a 3×3 cluster lying in a (0 0 1) plane is presented, with the black dotted line the outline of a bcc unit cell is shown. For further clarity the C atoms that lie on top of the (0 0 1) habit plane are slightly larger than those below. Figures b) to d) show a side-view of a part of the cluster; all figures show bonds between C atoms in the relaxed system shorter than 3 Å, atoms further from the observer are faded. In b) a part of the cluster is shown from the [1 0 0] direction, where the triangles formed by C atoms are visualized. In c) a part of the cluster is shown from the [0 1 0] direction, where the triangles are not visible. In d) a view from the [1 1 0] direction of a part of the cluster is given, where the triangles are visible. In e) a top-view of a part of the cluster is shown, where the Fe-C bonds with a length between 1.8 Å and 2 Å are shown in gray and yellow. A set of coordinates for 3D examination of an example cluster is provided in the supplemental data [24].

between C atoms and vacancies in the matrix, where for a vacancy and a C atom at a 1NN octahedral site the binding energy is found to be 0.89 eV using [12,13]. We also notice that some of the C atoms are bound less strong to the cluster, as some sites show a binding energy of just 0.57 eV. So C atoms can form a complex with a vacancy, the C-vacancy complex can then move away from a cluster.

The Fe atom (or vacancy) around which the C atoms are moved can be replaced by a M atom as in step 3a Fig. 3, this is not always energetically favorable, particularly for large M atoms like Nb. Alternatively the Fe atom in the cluster can be replaced by a vacancy. Hence the cluster acts as a 'vacancy sink'. Vacancies can then move through the cluster displacing M atoms to form a NaCl-structure locally, as depicted in Fig. 3 step 3b. Note that this immediately results in a Baker-Nutting orientation relation (BN-OR) [25–28]. The movement of C atoms, and the substitution of vacancies or M atoms can occur at the same time for different sites. In steps 4 and 5 of Fig. 3 snapshots are shown of the transforming cluster in which multiple sites are changed.

For smaller $FeMC_3$ clusters the substitution of Fe atoms with M atoms has an energetically unfavorable effect, the Fe atoms are rather replaced by vacancies. For larger clusters (larger than 7×7 Nb atoms, 5×5 Ti atoms) part of the Fe atoms can be substituted with M atoms. In the case of the 7×7 Nb cluster the gain in binding energy is 1.8 eV when substituting the center Fe atom, however the substitution of a second M atom is unfavorable as is the substitution of Nb atoms at other sites. Hence there is a dependence on the cluster size for the transformation, but also a dependence on the M atom size as for Ti this effect is weaker (see Table 6). This seems to be a size effect as Ti atoms are much smaller than Nb atoms, so the strain caused by Ti atoms is smaller than for Nb atoms. Hence Ti atoms have a better fit in the cluster.

The energetic favorability for the presence of vacancies in the $FeMC_3$ clusters and the role that they seemingly play in the movement of M atoms shows a parallel to the behavior of the Guinier-Preston zone in aluminum alloys [29,30], e.g., Al-Cu, and Al-Ag. In aluminum alloys the GP zone acts as a 'vacancy pump' [31,32], as the GP zone attracts vacancies (and vacancy-Cu complexes) there is a local accumulation of vacancies driving back vacancies into the matrix which in turn allows for the attraction of new M atoms as vacancies bind to the M atoms.

An attractive binding between first nearest-neighbor (1NN)

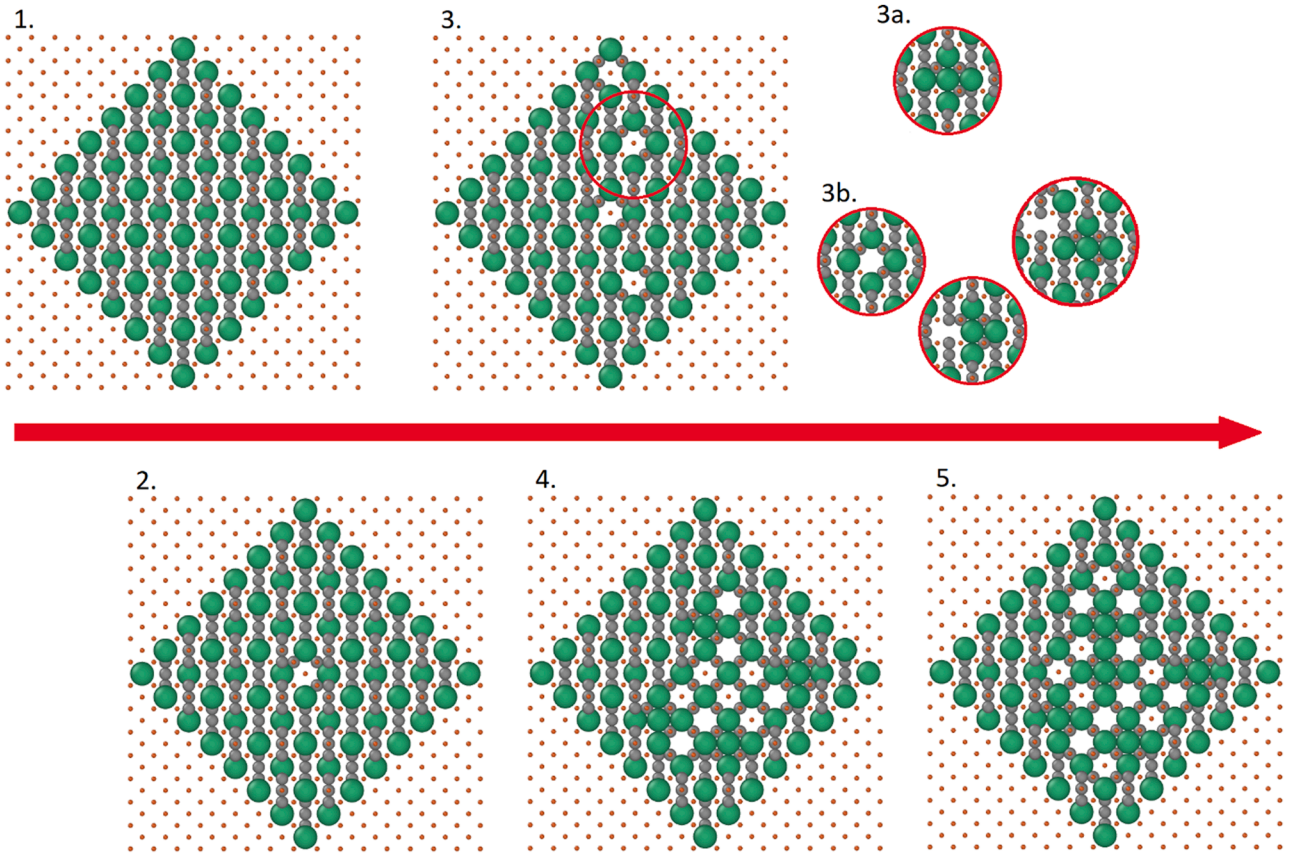

Fig. 3. A schematic overview of the transformation of a $FeMC_3$ cluster, for all steps a snapshot of an idealized representation of the cluster where the change is visible is provided. In step 1 an ideal $FeMC_3$ cluster is shown. In step 2 the C atoms around a single Fe site have moved into the 'NaCl-sites'. In step 3 multiple C atoms have moved into the 'NaCl-sites'. In steps 3a and 3b the two follow-up options are presented. In 3a a M atom has replaced the Fe atom at one of the sites, an alternative path is illustrated in 3b where the Fe atom is replaced by a vacancy. In 3b we also show that a neighboring M atom then moves into a (local) NaCl-structure where the vacancy migrates through the $FeMC_3$ cluster, note that the M atoms generally need to overcome a significant activation energy to migrate through the $FeMC_3$ cluster [11]. This process can be repeated where C atoms are moved into the habit plane, and vacancies or M atoms attach to the cluster to form a structure that locally has a NaCl-structure as shown in steps 4 and 5. Steps 4 and 5 show snapshots of the transformation of the cluster.

Table 5
Change in binding energy following transformation/relocation at the center atom of a $N \times N$ $FeNbC_3$ cluster (the site in Step 2. of Fig. 3). Various changes are checked and combined, such as the relocation of C atoms, the substitution of the Fe atom by a vacancy or a M atom, and finally the substitution with a vacancy and movement of a neighboring M atom with relocated C atoms. As the size of the cluster increases the favorability of the transformation is greater. Given the large change in binding energy for the relocation of C atoms, over 3 eV for a 6×6 cluster, the original $FeNbC_3$ structure is not expected to be maintained when the cluster reaches a size larger than 6×6.

Cluster size	2×2	4×4	6×6	8×8
Change $\Delta E_{bind.}$ [eV]				
Relocate C atoms	−0.64	−0.52	3.13	3.97
Replace Fe atom with vacancy	1.12	0.69	2.00	1.52
Relocate C atoms + replace Fe atom with vacancy	1.32	2.81	3.28	5.69
Replace Fe atom with Nb atom	−2.30	−0.33	1.20	−0.27
Relocate C atoms + replace Fe atom with Nb atom	−1.23	−1.65	0.99	2.71
Relocate C atom + substitute vacancy + move neighbor Nb atom	−0.65	−1.14	2.23	5.09

vacancies and M atoms in the ferrite matrix was observed in this study. For the used MEAM potentials we find 0.05 eV for Nb atoms and 1NN vacancies, and 0.13 eV for Ti atoms and 1NN vacancies [12,13]. A strong bond of 0.89 eV forms between a vacancy and a C atom at a 1NN

Table 6
Change in binding energy following transformation/relocation at the center atom of a $N \times N$ $FeTiC_3$ cluster (the site in Step 2. of Fig. 3). Various changes are checked and combined, such as the relocation of C atoms, the substitution of the Fe atom by a vacancy or a M atom, and finally the substitution with a vacancy and movement of a neighboring M atom with relocated C atoms. As the size of the cluster increases the favorability of the transformation is greater.

Cluster size	2×2	4×4	6×6	8×8
Change $\Delta E_{bind.}$ [eV]				
Relocate C atoms	−0.64	0.07	−2.08	2.74
Replace Fe atom with vacancy	−0.39	−0.54	−0.57	−0.30
Relocate C atoms + replace Fe atom with vacancy	−1.26	−0.43	0.57	3.42
Replace Fe atom with Ti atom	1.04	1.51	1.73	1.91
Relocate C atoms + replace Fe atom with Ti atom	1.28	0.65	1.34	5.56
Relocate C atom + substitute vacancy + move neighbor Ti atom	−1.66	−1.72	−2.82	2.80

octahedral site. DFT results show a stronger binding of 0.36 eV and 0.24 eV for with 1NN vacancies for Nb and Ti atoms respectively [32]. This confirms that the $FeMC_3$ cluster attracts vacancies and acts as a vacancy-sink.

To fully resemble the vacancy-pump described by Girifalco and Herman [31] the bond between M atoms and vacancies needs to be small, to be precise the binding of a complex needs to be weak near a $FeMC_3$ cluster, additionally the interaction between the $FeMC_3$ cluster

and the vacancy and between the $FeMC_3$ cluster and the complex needs to be small. The cluster has quite strong bonds with vacancies, so several vacancies will remain 'attached' to the cluster. However for vacancy complexes with C atoms there is a possibility that vacancies allow for transportation of excess C atoms away from a transformed cluster back into the matrix. So the cluster displays a partial resemblance of the GP zone, where we find a vacancy pump behavior, but instead the 'pumping' relies on the trade of M atoms for C atoms in vacancy complexes.

The relocation of the C atoms is favored near the center of the cluster, however the M atoms (particularly for Nb) are more easily added in 'NaCl-sites' near the edge. In the example of Fig. 3 substituting a Nb at the center site is unfavorable, as the total binding energy is lowered by 1 eV. Whereas substituting a Nb atom at the edge site (step 3a Fig. 3) is favorable, as the total binding energy increases by 0.6 eV. Secondly, the relocation of the C atoms around Fe sites (as in step 2 Fig. 3) favors the direction parallel to the 'rows' of C atoms, as displayed in step 3 of Fig. 3. As the cluster grows larger (in the habit plane) the number of M atoms that can be added in the planar cluster increases, both by substitution of Fe by M atoms in the cluster and by growth of the cluster at its edges. For example in a 5×5 $FeNbC_3$ cluster only the C atoms for a single Fe atom can be moved in an energetically favorable manner, but a Nb atom cannot be entered in a favorable way. For a 7×7 $FeNbC_3$ cluster the number of atoms that can be moved in a favorable manner is increased as can be seen in Fig. 3 step 4, where multiple Nb atoms (and vacancies) have been added whilst increasing the binding energy of the cluster by over 2 eV.

4.2. Matrix misfit and strain

Several factors may contribute to the change in cluster structure, but most notably the strain in the matrix, as the misfit between bcc Fe and NbC in the BN-OR is large and therefore causing an increase in total energy. For the MEAM potential there is an approximate 12 % misfit between the surface of the precipitate and the ferrite matrix, i.e., in the $\langle 1\,0\,0 \rangle$ directions parallel to the $\{1\,0\,0\}_\alpha$ plane in which the precipitate is situated, for the NbC [13] and approximately 9 % for TiC [18]. This impacts the coherency of the precipitate-matrix interface as observed by Sawada et al. [34]. For the NaCl-structure it has been found that NbC precipitates (multi layered cuboids) become semi-coherent at sizes above roughly 1.8 nm, for TiC this occurs at 3.6 nm [33]. Precipitates retain coherency longer, the more plate-like [35], as also observed in the current work where none of the studied clusters, of which the largest is a 11×11 M atom cluster (4.5 nm) consisting of a single layer, lost its coherency when fully relaxed.

The $FeMC_3$ cluster and the partially transformed clusters have a better fit with the bcc lattice than the NaCl-structured MC. $FeMC_3$ clusters display anisotropy in their lattice parameter. We relax the $\{1\,0\,0\}$ plane, and the $\{2\,0\,0\}$ planes containing the M and C atoms to find approximate lattice parameters, for $FeNbC_3$ the lattice parameter parallel to the C atom rows is 2.98 Å and 3.08 Å perpendicular to the rows, and for $FeTiC_3$ the lattice parameter parallel to the C rows is 2.93 Å and 3.03 Å perpendicular. There are much smaller misfits than for the NbC and TiC carbides at just 4 % parallel and 7 % perpendicular (to the C rows) for $FeNbC_3$, and 2 % parallel and 6 % perpendicular for $FeTiC_3$. It has been suggested that the strain in the direction perpendicular to the habit plane of the precipitate is the root cause for the transformation to NaCl-structured carbides [8]. In this work it is observed that in the $\{1\,0\,0\}$ planes parallel to the cluster the Fe atoms are displaced outward perpendicular to the habit plane of the cluster (tensile strain), this strain is lowered with the transition to MC for larger clusters, which is displayed in Fig. 4.

In Fig. 4c and 4d C atoms are moved into the 'NaCl-sites' to

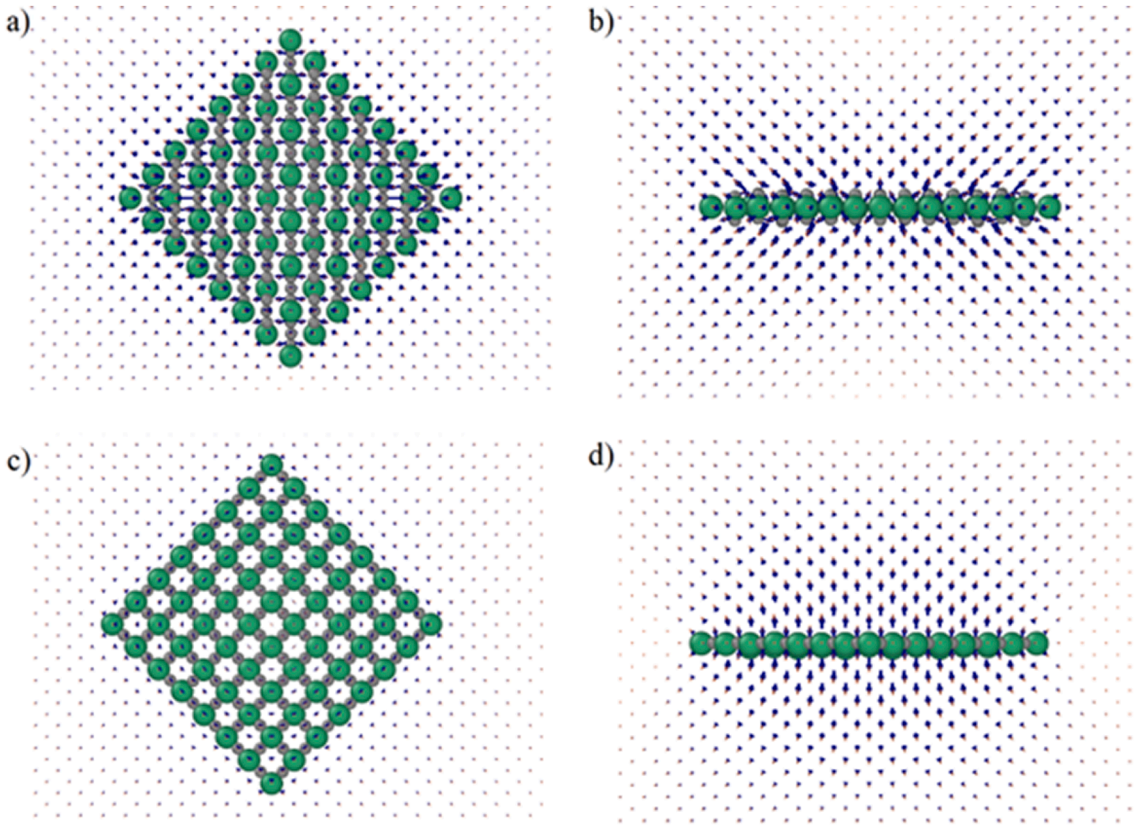

Fig. 4. Displacement of Fe atoms in the matrix from their bcc equilibrium positions. The green (largest) atoms are the M atoms, and the grey (mid-sized) atoms are C atoms, and the smallest atoms are the Fe atoms. Idealized $(Fe,M)C_3$ cluster a) top-view, b) side view. The platelet with relocated (and some removed) C atoms still containing high a fraction of Fe c) top-view, d) side view. Fe atoms for the $FeMC_3$ cluster, a) and b), are displaced in the $\langle 1\,1\,0 \rangle$ directions out of the habit plane. For the platelet with relocated C atoms, c) and d), Fe atoms are displaced in the $\langle 1\,0\,0 \rangle$ direction perpendicular to the habit plane.

demonstrate the effect on the displacement in the matrix without interference with other effects, e.g., vacancies, substitution of Fe atoms by M atoms etc. Note that besides moving C atoms several C atoms are also removed in Fig. 4c and 4d. The real transformation occurs in steps and only for parts of the cluster as presented in Fig. 3, which is discussed above.

The displacement in the surrounding ferrite matrix caused by the original $FeMC_3$ cluster is in large parts directed in ⟨1 1 0⟩ directions, whereas the displacement by a NaCl-structured {1 0 0} platelet is primarily directed in the ⟨0 0 1⟩ directions. The driving force behind the transformation from $FeMC_3$ to MC can be understood from the strain energy density in the matrix associated with these two directions, f^{hkl}_{strain}, as adapted from [35].

$$f^{hkl}_{strain} = 2\varepsilon^2 Y(hkl). \tag{3}$$

Where *hkl* indicates the direction of the strain, ε is the magnitude of the strain given by $\varepsilon = (a - a_0)/a_0$ where a_0 is the equilibrium lattice parameter, and a the strained lattice parameter. Finally $Y(hkl)$ is the associated elastic constant. To get an energy (per atom) rather than an energy density Eq. (3) is integrated over the atomic volume of the equilibrium state:

$$E^{hkl}_{strain} = 2\varepsilon^2 Y(hkl) V_{at}. \tag{4}$$

Where V_{at} is the atomic volume in the equilibrium state. From [36] the elastic constants can be found for different directions:

$$Y(100) = \frac{(C_{11} + 2C_{12})(C_{11} - C_{12})}{C_{11}}, \text{and} Y(110) = \frac{3(C_{11} + 2 \bullet C_{12})(C_{11} - C_{12} + 4C_{44})}{5C_{11} - 4C_{12} + 8C_{44}}. \tag{5}$$

Here C_{ij} are the elastic parameters in Voigt notation. For iron, as used in the MEAM potential [12,13], $Y(100) = 224$ GPa and $Y(110) = 337$ GPa. The main strain contribution comes from the ferrite matrix, as it is observed in simulations performed in this study that clusters consisting of a single layer conform to the matrix lattice to form a highly coherent interface. The M atoms are displaced out of the habit plane to form a wave-like pattern (Fig. 5) whilst still forming a single atom layer. This is quite similar to the rippling observed in Fe/MC interfaces seen by Jung et al. [37] except that there are no bulk MC layers in the simulations performed in this work.

In simulations, of the two clusters depicted in Fig. 4, for Fe-Nb-C it is established that the strain varies greatly along the surface of the formed $FeMC_3$ and MC cluster. The largest strain occurs toward the edges of the cluster. Using the displacement in the direct neighboring {1 0 0} planes parallel to the habit plane the strain energy is calculated using Eq. (4), the clusters depicted in Fig. 4 are used. For the $FeMC_3$ cluster the strain energy density is roughly 1.6 eV per Fe (in the first adjacent {1 0 0} plane) atom based on an average displacement of 0.4 Å in the ⟨1 0 0⟩ direction and 0.4 Å in the ⟨1 1 0⟩ direction, for the MC cluster the strain energy density is 1.0 eV per Fe atom based on the average displacement of 0.5 Å in the ⟨1 0 0⟩ direction. A similar trend is seen for the Fe-Ti-C system. Here it is noted that these strain energies are very high, so in real clusters we expect the transformation, as described above, to start in much smaller precipitates.

4.3. Results from LAMMPS simulations

In Fig. 3 the transformation of a $FeMC_3$ cluster is shown, where various steps in the transformation are highlighted. Static relaxations of these steps in $FeMC_3$ clusters using LAMMPS for $FeNbC_3$ and $FeTiC_3$ show that the transformation occurs in steps, in these steps the binding energy of the cluster is increased. Initially the C atoms migrate to the octahedral interstitial sites in the habit plane, in the same step the Fe atoms can be replaced by vacancies. This movement of C atoms and the introduction of vacancies may occur for various sites in the {1 0 0} habit plane of the $FeMC_3$ cluster. At the sites where the C atoms have rearranged into the habit plane, i.e., the 'NaCl-sites', a M atom can substitute an Fe atom or a vacancy. All these steps occur in an energetically favorable manner. The $FeMC_3$ cluster contains a high C atom fraction, it must be noted that these C atoms may (re-)attach to a M–C cluster or dissolve back into the matrix after the transformation. Generally C atoms are still (weakly) bound to the NaCl-structured platelet, however we note that some of the weakly bound C atoms form strong bonds with vacancies and can move away from a cluster via a C-vacancy complex.

We note that the $FeNbC_3$ cluster allows many vacancies within the cluster, for $FeTiC_3$ the number of vacancies is much lower. The main reason behind this seems to be the size difference between Nb and Ti atoms in ferrite [22], Nb atoms are much larger and cause more strain in their neighborhood. Note that this coincides with the DFT results in Section 3, where large M atoms also display much less favorable (or even unfavorable) pair interactions with other M atoms or C atoms.

Thus the transformation occurs in steps, moreover the extent of the transformation depends on the cluster size. Small clusters cannot transform in an energetically favorable manner, but for larger clusters the transformation does increase the binding energy of the cluster.

The main driving force for the transformation is determined to be the matrix strain caused by the $FeMC_3$ cluster, in directions perpendicular to the habit plane of the cluster. A $FeMC_3$ cluster on the {1 0 0} habit plane causes a strain in the [1 1 0] and [1–10] directions in the ferrite matrix, whereas the MC platelet primarily causes a strain in the [1 0 0] direction. The strain in ⟨1 0 0⟩ directions causes a lower strain energy than the strain in the ⟨1 1 0⟩ directions.

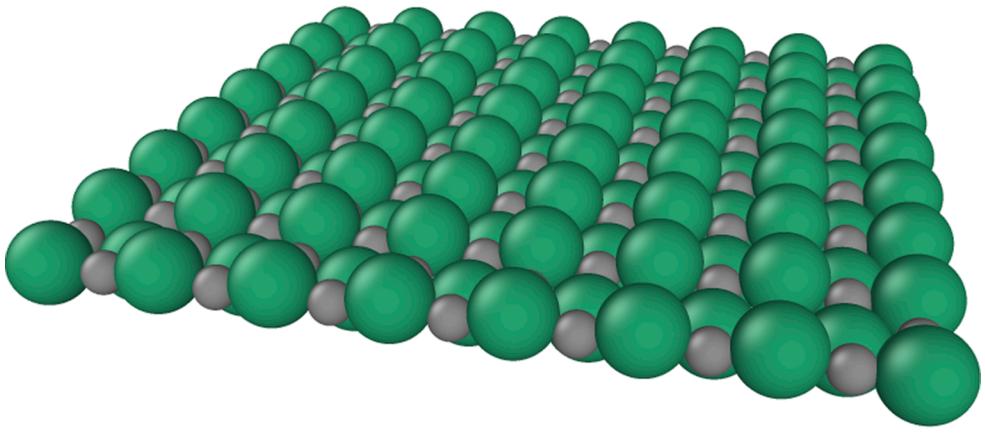

Fig. 5. A single atomic layer of NbC where the Nb atoms are pushed out of the (1 0 0) habit plane of the platelet. The Nb atoms form a wave-like pattern where one half is pushed up, and the other half is pushed down.

The transformation, as described in Section 4.1 and illustrated in Fig. 3, is energetically favorable, hence the replacement and relocations of atoms in the transformation may occur simultaneously. The LAMMPS simulations further suggest that the $FeMC_3$ clusters act in a similar manner as GP zones in aluminum alloys [31,32], where the GP zone attracts vacancies and the precipitate forming elements are bound to vacancies, which is also the case for the Nb and Ti atoms as verified in this study. As the precipitate forming atoms are attracted to vacancies, and the vacancies are attracted by the GP zone more precipitate forming atoms are attracted to the GP zone, where the GP zone acts as a weak 'vacancy pump' [31]. But in the case of these carbides the excess C atoms are necessary in the return of vacancies to the matrix.

The cluster size at which the transformation occurs is found to be 3 nm for $FeNbC_3$ and 2 nm for $FeTiC_3$. Courtois et al. [5] find platelets of Nb(C,N) precipitates with an average size 3 nm using TEM, and 8 nm using High-Resolution TEM. Breen et al. [6] find Nb(C,N) platelets as small as 3 nm. Wang et al. [8] find (Ti,Mo)C platelets of sizes 1.5 nm, which they call embryo clusters, as these small cluster have not fully taken to NaCl-structure, which occurs at sizes of 6 nm and larger. So the simulation results are in agreement with the experimental results.

Experimental clusters however show a lower carbon concentration for the Carbide clusters, in part this is due to the presence of N atoms. Additionally we note that C atoms have a higher mobility than the M atoms and can therefore move away from the $FeMC_3$ cluster during the transformation.

The current study does not provide a time-scale at which the transformation takes place. Experimental studies [5–8] indicate that platelets can form in 10^1 to 10^2 seconds, the timescale depends strongly on temperature, e.g., [6]. Therefore it may be difficult to observe a $FeMC_3$ cluster, as they transform already at small sizes (3 nm for $FeNbC_3$, 2 nm for $FeTiC_3$) to MC platelets. Furthermore we have found that $FeMC_3$ clusters are highly coherent with the ferrite matrix making detection harder.

5. Conclusion

The pair interactions of M atoms, where M = Ti, Zr, Hf, V, Nb, Ta, in M–M pairs and M–C pairs embedded in ferrite display a same pattern for all studied metals. Indicating that the transition metal carbides all form in a similar manner. M atoms attach to a C atom cluster in ferrite in which an ordered $FeMC_3$ cluster forms in a {1 0 0} oriented lattice plane of the ferrite matrix. Here the M atoms form a checkerboard pattern with Fe atoms in a single {1 0 0} plane, this Fe-M structure is surrounded by C atoms.

The clusters that form initially do not have the NaCl-structure, but rather a $FeMC_3$ stoichiometry containing a large Fe fraction. The results from our simulations show that the transformation occurs through several energetically favorable steps in which vacancies seem to play a significant role. The role of vacancies and the $FeMC_3$ clusters appears similar to that of GP zones in aluminum alloys.

Furthermore the in-plane transformation to NaCl-structured platelets is found to be driven by the strain directed in the directions perpendicular to the habit plane of the cluster/precipitate, i.e., in the (1 0 0) planes neighboring the habit plane.

The formation and transformation of $FeMC_3$ clusters presented here provide the theoretical basis that clarifies experimentally observed carbide platelet nucleation and (early) growth.

CRediT authorship contribution statement

R.J. Slooter: Writing – review & editing, Writing – original draft, Visualization, Methodology, Investigation, Formal analysis, Data curation, Conceptualization. **M.H.F. Sluiter:** Writing – review & editing, Validation, Supervision, Software, Resources, Project administration, Methodology, Investigation, Funding acquisition, Formal analysis, Data curation, Conceptualization. **W.G.T. Kranendonk:** Writing – review & editing, Validation, Supervision, Resources, Investigation, Formal analysis, Conceptualization. **C. Bos:** Writing – review & editing, Validation, Supervision, Formal analysis, Conceptualization.

Declaration of competing interest

The authors declare that they have no known competing financial interests or personal relationships that could have appeared to influence the work reported in this paper.

Data availability

Data will be made available on request.

Acknowledgements

This research was carried out under project number T17019m in the framework of the Research Program of the Materials Innovation Institute (M2i) supported by the Dutch government.

Appendix A. Supplementary data

Supplementary data to this article can be found online at https://doi.org/10.1016/j.commatsci.2024.113097.

References

[1] M. Volmer, A. Weber, Z. Phys, Chem. 119 (1926) 277–301.
[2] R. Becker, W. Döring, Annalen Der Physik 416 (1935) 719–752.
[3] R. Kampmann, R. Wagner, Decomposition of alloys: the early stages, Pergamon Press (1984) 91–103.
[4] M. Perez, M. Dumont, D. Acevedo-Reyes, Acta Mater. 56 (2008) 2119.
[5] E. Courtois, T. Epicier, C. Scott, Mater. Sci. Forum 500–501 (2005) 669–676.
[6] A.J. Breen, K.Y. Xie, M.P. Moody, B. Gault, H.-W. Yen, C.C. Wong, J.M. Cairney, S. P. Ringer, Microsc. Micranal. 20 (2014) 1100–1110.
[7] J. Takahashi, K. Kawakami, Y. Kobayashi, Acta Mater. 153 (2018) 193–204.
[8] J. Wang, M. Weyland, I. Bikmukhametov, M.K. Miller, P.D. Hodgson, I. Timokhina, Scripta Mater. 160 (2019) 53–57.
[9] X. Zhang, C. Ioannidou, G.H. ten Brink, A. Navarro-López, J. Wormann, J. Campaniello, R.M. Dalgliesh, A.A. van Well, S.E. Offerman, W.G.T. Kranendonk, B.J. Kooi, Mater. Design. 192 (2020) 108720.
[10] C. Ioannidou, A. Navarro-López, A. Rijkenberg, R.M. Dalgliesh, S. Koelling, C. Pappas, J. Sietsma, A.A. van Well, S.E. Offerman, Acta Mater. 201 (2020) 217–230.
[11] R.J. Slooter, M.H.F. Sluiter, W.G.T. Kranendonk, C. Bos, Comp. Mat. Sci. 230 (2023) 112455.
[12] H.-K. Kim, W.-S. Jung, B.-J. Lee, Acta Mater. 57 (2009) 3140–3147.
[13] H.-K. Kim, W.-S. Jung, B.-J. Lee, J. Mater. Res. 25 (7) (2010) 1288–1297.
[14] M.H.F. Sluiter, Materials Research Society symposia Proceedings, 979(2006), art. No. 1403.
[15] A.P. Thompson, H. Metin Aktulga, R. Berger, D.S. Bolintineanu, W. Michael Brown, P.S. Crozier, P.J. in 't Veld, A. Kohlmeyer, S.G. Moore, T.D. Nguyen, R. Shan, M.J. Stevens, J. Tranchida, C. Trott, S.J. Plimpton, Comp. Phys. Comm., 271(2022), 108171.
[16] D. A. Porter, K. E. Easterling, and M. Y. Sherif, Phase Transformations in Metals and Alloys, Third Edition, CRC Press, pp. 288-302.
[17] G. Kresse, J. Hafner, Phys. Rev. B 47 (1993) 558.
[18] G. Kresse, J. Hafner, Phys. Rev. B, 49(1994), 14 251-269.
[19] G. Kresse, J. Furthmüller, Comp. Mat. Sci. 6 (1996) 15.
[20] G. Kresse, J. Furthmüller, Phys. Rev. B, 54(1996), 11 169-186.
[21] G. Kresse, D. Joubert, Phys. Rev. 59 (1999) 1758.
[22] C.K. Ande, M.H.F. Sluiter, Metal. Mater. Trans. A 43 (2012) 4436–4444.
[23] W.-S. Jung, S.-H. Chung, Modelling Simul. Mater. Sci. Eng. 18 (2010) 075008.
[24] Supplemental data available at [URL].
[25] R.G. Baker, J. Nutting, I.S.I. Spec, Rep. 64 (1959) 1.
[26] R.M. Smith, D.P. Dunne, Mater. Forum (rushcutters Bay) 11 (1988) 166–181.
[27] F. Ishikawa, T. Takahashi, T. Ochi, Metall. Mater. Trans. A 25 (1994) 929–936.
[28] Z.-G. Yang, M. Enomoto, Mater. Sci. Eng. 332 (2002) 184–192.
[29] A. Guinier, C.R. Acad, Sci. 206 (1938) 1374–1376.
[30] G.D. Preston, Phil. Mag. 26 (1938) 1355–1371.
[31] L.A. Girifalco, H. Herman, Acta Metall. 13 (1965) 583–590.
[32] M.V. Petrik, Y.N. Gornostyrev, P.A. Korzhavyi, Scripta Mater. 165 (2019) 123–127.
[33] C.D. Versteylen, N.H. van Dijk, M.H.F. Sluiter, Phys. Rev. B 96 (2017) 094105.
[34] H. Sawada, S. Taniguchi, K. Kawakami, T. Ozaki, Metals 7 (2017) 277–289.
[35] H. Sawada, S. Taniguchi, K. Kawakami, T. Ozaki, Model. Simul. Mater. Sci. Eng. 21 (2013) 045012.
[36] J.W. Cahn, Acta Metall. 10 (1962) 179–183.
[37] W.-S. Jung, S.-C. Lee, S.-H. Chung, ISIJ Int. 48 (2008) 1280–1284.